Defect detection with generative adversarial networks for electroluminescence images of solar cells

Chunhui Shou, Ling Hong, Waner Ding, Qu Shen
Zhejiang Provincial Key Laboratory of Solar Energy Utilization & Energy Saving Technology, Zhejiang Energy Group R&D
Hangzhou, China
shouch@zjentc.com, hongl@zjentc.com, dingwe@zjentc.com, qu.shen@outlook.com

Wenhao Zhou, Yu Jiang, Chunhui Zhao*
State Key Laboratory of Industrial Control Technology
College of Control Science and Engineering, Zhejiang University
Hangzhou, China
3160104366@zju.edu.cn, jy0514@zju.edu.cn, chhzhao@zju.edu.cn(*corresponding author)

2020 35th Youth Academic Annual Conference of Chinese Association of Automation (YAC) | 978-1-7281-7684-0/20/$31.00 ©2020 IEEE | DOI: 10.1109/YAC51587.2020.9337676

***Abstract*—Solar cells are the core module of photovoltaic (PV) modules. Defects will decrease the power efficiency of solar cells and reduce the stability of PV power systems. Electroluminescence (EL) imaging is able to image solar modules with higher resolution so that defects can be better detected. The current manual detection of EL images is slow and requires relevant expertise, so methods based on computer vision for automatic detection in EL images are appearing. However, due to the heterogeneously background of the EL images and the lack of defect samples, automatic detection of defects has been a challenging task. We design a model based on generative adversarial networks (GAN) and auto-encoder (AE) to perform defect detection for EL images of solar cells. It only requires normal images in the training process and detect defects by measuring the residuals between the test image and the constructed image generated by the generator. To reduce the effects of image distortion, we combine structural similarity index (SSIM) with feature residuals to train the encoder, which can get better results than the model using typical mean square error (MSE). During the detection phase, SSIM and MSE are combined as the anomaly score. Our method has higher recognition of defective EL images and achieves detection accuracy of 90.0% on the test set. Compared with the method using only MSE, the F1 score is increased obviously.**

Keywords—solar cells; deep learning; defect detection; generative adversarial network

I. INTRODUCTION

Solar cells are the core modules of photovoltaic (PV) modules. Solar cells are protected from the environment by aluminum frames and glass laminates. However, these protection measures do not always prevent mechanical damage such as falling PV modules during installation. And because the silicon wafer of the solar cell is thin, it is easy to cause the crack of the silicon wafer. Cracks will reduce the stability, reliability and service life of PV modules, ultimately affect the efficiency of the PV system. So, it is very important to ensure the quality of solar cells for PV modules.

Current manual defect detection methods require experienced experts to inspect the solar cell images to identify defects, which can only be quantitatively sampled and cannot fully detect all solar cells. Moreover, experts mainly detect solar cell images where some small cracks inside the crystal surface cannot be effectively detected expect the obvious cracks on the glass. Therefore, the solar cell detection technology based on machine vision has great application scenarios.

Electroluminescence (EL) imaging is a mature, non-destructive technology that captures near-infrared images with wavelengths from 950nm to 1250nm, enabling imaging solar module with higher resolution. Defective cells are darker in EL images and cracks appear as dark curves and complex geometries enabling the detection of microcracks. However, the discrimination between the defect areas and the background is low and some grains that appear in a curved shape might be mistaken for cracks. In addition to cracks, the defects of solar cells also include dark spots, material defects and electrically insulation. Therefore, defect detection of solar cells is a challenging task.

Recently, anomaly detection methods based on deep learning have been applied to various fields [1][2]. Research on the detection of solar cells based is active, but the related work mostly focused on detecting cracks in solar cells. Chen et al. [3] proposed a crack detection scheme for multicrystalline solar cells. This method generates crack saliency map by steerable evidence filtering and extracts crack by local threshold and minimum spanning tree. This method can partially eliminate the influence of background noise and improve the accuracy of crack detection. However, only lower-dimensional features can be detected and some high-dimensional complex features cannot be effectively extracted.

Tsai et al. [4] proposed a independent component analysis (ICA) based method which involves a learning and a detection stage. By means of ICA, a set of independent basis images are detected by normal solar cell images. Each solar cell image is reconstructed as a linear combination of the detected images. While it achieves a high recognition rate, it cannot discriminate defect types and locate defects.

Based on the ideal P-N junction model, Wang et al. [5] simulated the relationship between the EL intensity and carrier diffusion length. The relationship between the defects of solar cells and the diffusion length of minority carriers is summarized then the defects can be detected in theory. However, this method is susceptible to external and background influences.

Tsai et al. [6] proposed a Fourier image reconstruction method based self-reference scheme for the detection of solar cell EL images. Fourier image reconstruction is applied to remove the defects in the image by making the corresponding components to 0. It is inefficient to detect complex defects.

Tsai et al. [7] also proposed an anisotropic diffusion scheme to detect cracks in solar cell images. The diffusion coefficients is adjusted by taking gradient and gray scale as features. Anwar et al. [8] presented a method for the micro crack detection in solar cell images. The anisotropic diffusion filter and image segmentation technology are used in this method. Although these methods perform well in detecting microcracks, they do not take into account other defect types and are susceptible to influence of grain in the background.

Different from the traditional method of manually extracting features, the deep learning algorithm has a strong ability to automatically extract features, which is a current research hotspot. However, there is less research on applying deep learning to EL images of solar cells. Deitsch et al. [9] proposed a SVM classifier that can be used with low computational requirements and a supervised convolutional neural networks (CNN) that GPUs are required in the training process. This method predicts the likelihood of defects for each PV module. Zhang et al. [10] applied a supervised deep CNN to pavement cracks detection which is more effective than hand-craft methods. Chen et al. [11] proposed a CNN-based deep learning framework and a Naïve Bayes data fusion scheme for defect detection from the individual video frames of nuclear power plants. Jing et al. [12] proposed a fabric defect classification CNN method based on modified AlexNet. Cha et al. [13] developed a classifier for detecting concrete cracks from civil infrastructure images by using CNN. However, these algorithms require abundant labeled defect images and cannot locate the location of the defect.

To overcome the problem of sparse defect samples and difficult manual labeling, many unsupervised anomaly detection algorithms based on generative adversarial networks (GAN) [14] have been proposed. Akcay et al. [15] used a conditional GAN that learns the mapping of the data spaceand the mapping of the latent space. It employed the encoder-decoder-encoder structure in the generator network to reconstruct the output image. Zenati et al. [16] trained a BiGAN-based model to simultaneously learn an encoder along with a generator and discriminator, which enables avoiding the process of mapping to the latent space at inference. Thomas et al. [17] applied GAN to clinical imaging, which uses WGAN to generate normal image distribution and uses an encoder to learn the mapping from the image space to the latent space. By comparing the original image differences from the generated image to determine the abnormality. These methods only require normal samples for training, but when comparing images, they just use the mean square error (MSE) of the pixels between images as the loss function. Since the generator cannot accurately describe the normal data, using MSE will cause image distortion.

In the present work, we propose a solar cell defect detection method based on unsupervised deep learning, which has high accuracy and real-time performance. To solve the problems of lack of defect samples and difficult sample labeling, a GAN-based unsupervised anomaly detection algorithm is developed to detect defects for solar cell EL images. In order to reduce the impact of image distortion, structural similarity index (SSIM) is calculated to describe the differences between origin images and constructed images. The proposed method only requires normal solar cell EL images for training, and can detect and locate different defects of solar cells.

The remainder of this paper is organized as follows. The proposed methodology is described in Section II. The experimental settings, comparison results, and corresponding analysis are provided in Section III. Finally, Section IV concludes the paper.

II. METHODOLOGY

GAN is an unsupervised deep learning method, first proposed by Goodfellow [14]. The original purpose of GAN was to generate images close to the real image. GAN includes two networks, namely a generator network and a discriminator network. The generator is used to generate images and the discriminator learns to judge whether samples come from the generated distribution or the real data distribution. The generator learns a mapping from the latent space to the real data space and learns the real data distribution. A discriminator is usually a classification network structure. The original GAN has the difficulty of training. After continuous development, many different GAN improvement algorithms have been proposed. Among them, WGAN-GP [19] uses wasserstein distance as the loss function and the training performance of GAN is greatly improved.

The autoencoder (AE) consists of an encoder and a decoder. The encoder maps the data space to the latent space, then the decoder maps the latent space back to the data space. AE can be regarded as a feature detector and can get efficient feartures of the input data. Zheng et al. [20] developed a method based on GAN to detect telecom fraud. A deep denoising AE learns the probabilistic relationship between the input features, and distinguish positive samples and negative samples in data distribution by adversarial training.

The network structure of our GAN-based unsupervised anomaly detection method is similar to [17], which includes a GAN and an encoder. However, our GAN structure adopts a WGAN-GP structure with better training performance and we do not need to split the solar cell EL image into patches. First, we train a GAN network based on normal solar cell EL images to get a generator and a discriminator. Then based on the trained GAN network, we train an encoder to map the image to its corresponding latent space. In the detection phase, we use the encoder to get the corresponding latent space of the test image. Then use the generator in the GAN network to transform the latent space back to its corresponding image space. By

measuring the residuals between the original image and the constructed image, an abnormal score is obtained to determine whether it is an abnormal image.

Next, we describe the specific training process of GAN and the encoder, then describe the image anomaly detection process by constructing the anomaly score.

A. *Training the WGAN-GP with normal images*

We train a WGAN-GP using normal solar cell images with distribution of p_{data}. WGAN-GP uses the wasserstein distance as the criterion for measuring the differences between two distributions. The structure of WGAN-GP training is shown in Fig. 1.

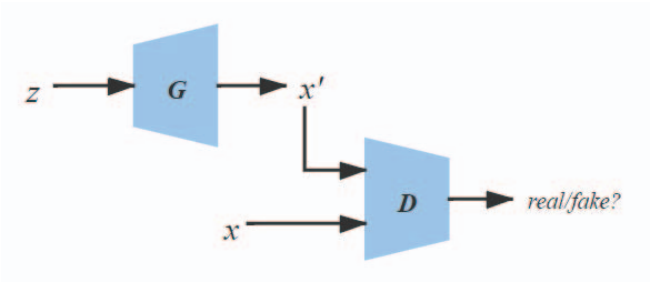

Fig. 1. The structure of WGAN-GP training

The generator G learns the distribution of p_g over data x via a mapping $G(z)$ of samples z. The corresponding loss function of G is:

$$Loss_G = -E_{x\sim p_g}[D(x)] \quad (1)$$

WGAN-GP utilizes gradient penalty to limit the gradient of discriminator D to not exceed K. It does not sample the entire space, but only samples the space $p_{\hat{x}}$ between p_{data} and p_g. Its loss function is:

$$Loss_D = E_{x\sim p_g}[D(x)] - E_{x\sim p_{data}}[D(x)] + \lambda E_{x\sim p_{\hat{x}}}\left[\|\nabla_x D(x)\|_p - K\right]^2 \quad (2)$$

Adversarial methods are used to optimize the discriminator and generator alternately. D is trained to maximize the probability of distinguishing training images and images generated from G. The generator is trained to be able to deceive the discriminator as much as possible, so that the generated image is close to the real image. After training, we can get a generator from WGAN-GP, which represents the mapping from latent space to image space, acting as a decoder, and a discriminator as the feature extractor.

B. *Training the encoder to learn the mapping from the image space to the latent space*

We can get a generator G from WGAN-GP to map the latent space to the image space. However, when performing defect detection, we also need an encoder which maps the image space x to the latent space z. [21] finds the latent space z corresponding to the image by the iterative process. It defines an alternative discrimination loss to measure the dissimilarity between query images and constructed images. However, the iterative process is time-consuming, which is not suitable for use in actual scenarios.

Referring to the structure of AE, we put the trainable encoder E into the structure of the autoencoder and the trained generator was treated as the decoder by fixing its parameters. There are mainly two structures for encoder training.

The first reverses the order of encoder and decoder. During the training process, it randomly samples in the latent space z, obtains the corresponding image space through a fixed parameter generator, then the encoder maps the image back to its latent space. That is, it is a $z - image - z$ structure where the decoder is before the encoder. The encoder is trained by minimizing the MSE of input z and reconstructed z. However, the disadvantage of this approach is that the encoder only receives input to constructed images during training without the participation of real images. Because the constructed image and the origin image will necessarily have a certain difference, this will cause the generator's mapping ability to the real image to be insufficient.

The second is a standard AE structure. During training, we use the same normal image as when training WGAN-GP as the input of the AE and get the latent space z corresponding to the image through the trainable encoder E. Then input z into the generator with fixed parameters to get its corresponding image space, Fig. 2 is the schematic diagram of the structure. We train the encoder E by minimizing the residuals between the original image and the final constructed image. Because it uses real samples for training, it can reflect the mapping from real images to latent space. In this paper, we have adopted this standard AE structure.

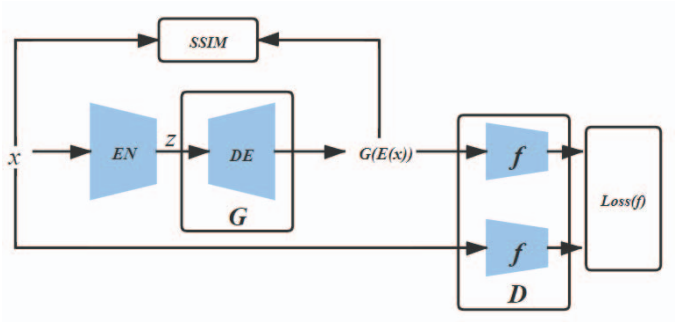

Fig. 2. The structure of encoder training

When comparing the differences between images, the general method is to directly compare the MSE between the pixels of images. However, in our scenario, because the image generated by the generator does not fully represent the normal image data distribution, the final generated image will definitely be different from the original image when training with normal images. At this time, the comparison between pixels cannot fully reflect the differences between images. At the same time, when the two images are very different, such as light and dark differences in some areas, the MSE between the pixels may also be the same. Therefore, we propose using SSIM [18] as the criterion for measuring the differences between images. The SSIM measures the difference between images as a whole which is more in line with human visual system.

However, only using the differences between images as the loss function has a disadvantage which will make the encoder focus on making the generated image as close as possible to the

original image. Because our generator is trained from a specific distribution of latent space (Gaussian distribution), this may cause the latent space of the encoder output not match the distribution of the generator's input, resulting in the generated image is not always normal image. To prevent this, we use the discriminator D in WGAN-GP as a feature extractor to get the high-dimensional features of the original image and the generated image. By minimizing the feature residues of the two images in the penultimate layer of the discriminator to ensure that the generated image is normal. Finally, the loss function of encoder is the sum of the inverse of SSIM between the images and the residuals of features extracted by the discriminator:

$$Loss_E = -\frac{k_1}{n_i} SSIM\left(x, G\big(E(x)\big)\right) + \frac{k_2}{n_f} Loss_f(x, G(E(x))) \quad (3)$$

$$SSIM(x, G(E(x))) = \frac{\left(2\mu_x\mu_{G(E(x))}+c_1\right)\left(2\sigma_{xG(E(x))}+c_2\right)}{\left(\mu_x^2+\mu_{G(E(x))}^2+c_1\right)\left(\sigma_x^2+\sigma_{G(E(x))}^2+c_2\right)} \quad (4)$$

$$Loss_f(x, G(E(x))) = \left\| f(x) - f\left(G\big(E(x)\big)\right)\right\|^2 \quad (5)$$

Where n_i is the number of pixels of the image and n_f is the dimensionality of the penultimate feature representation and $f(*)$ represents the penultimate layer of the discriminator.

C. Anomaly detection process.

In the anomaly detection phase, we first determine whether the test image is an anomaly image. If it is an anomaly image, we also need to locate the anomaly area. The specific detection process is to input the test image into the encoder E to obtain its latent space, then input the latent space to the generator to obtain its corresponding normal image. In order to determine whether the test image is normal, we define an anomaly score to measure the degree of abnormality of the image. The anomaly score refers to the loss function of the encoder which consider the differences between the two images and their feature residuals at the same time. Because SSIM measures the difference between two images as a whole, it has insufficient ability to detect small defects. In order to detect the tiny defects, we use MSE as the criterion to evaluate the difference between images. Then the anomaly score is:

$$A(x) = -\frac{k_1}{n_i}\left\|x - G\big(E(x)\big)\right\|^2 + \frac{k_2}{n_f}\left\| f(x) - f\left(G\big(E(x)\big)\right)\right\|^2 \quad (6)$$

However, because we are using SSIM as the loss function to train the encoder, using MSE alone as the evaluation standard will result in higher errors and MSE will accumulate small errors between pixels. So, we use a combination of MSE and SSIM as part of the anomaly score:

$$A(x) = -\frac{k_1}{n_i}\frac{\left\|x - G\big(E(x)\big)\right\|^2}{SSIM\left(x, G\big(E(x)\big)\right)} + \frac{k_2}{n_f}\left\| f(x) - f\left(G\big(E(x)\big)\right)\right\|^2 \quad (7)$$

Equation (7) adds SSIM to the overall measurement based on MSE. In this way, the accumulation of inter-pixel error with MSE can be corrected as a whole and also meets our training standards.

If the test image is a normal image, the corresponding image obtained through the AE will be very similar to it, so its anomaly score will be low; if the test image is an abnormal image, since the AE always outputs its corresponding normal image, so its anomaly score will be high. We obtain a threshold for anomaly scores based on the whole normal images used for training. When the anomaly score is greater than this threshold, it is judged as an abnormal image. At this time, we can compare the differences between the abnormal image and the constructed image obtained by the AE to locate the abnormal area.

III. Experiments

We prepare 584 EL images of normal solar cells with 300×300 pixels and 197 EL images of abnormal solar cells, which include different types of abnormalities such as cracks, breaks and dark spots (Fig. 3). Among them, 513 normal images are used as the training set of WGAN-GP and encoder, 71 normal images and 197 abnormal images constitute the test set. In order to illustrate the effectiveness of our model, we need to evaluate whether when given a test image, our model can generate normal images corresponding to it, and whether our model can detect abnormal images and locate abnormal areas. Both SSIM and MSE are used in the encoder's loss function to compare the effects between them. Meanwhile, different anomaly score types (6) and (7) are used in the detection phase.

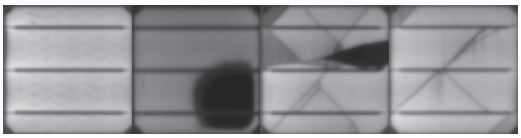

(a) (b) (c) (d)

Fig. 3. The plot of EL images for (a)normal case, (b)material defect, (c) electrically insulated cell parts, and (d)crack

A. Results

ResNet are utilized as the backbone structure of WGAN-GP and encoder, each comprising four residual blocks. We use a 3×3 convolution kernel with a stride of 1 and the activation function is RELU. We adopt Adam as a stochastic optimizer. We train the WGAN-GP model with 2000 epochs and 1000 encoder training epochs. We simply make $k_1 = k_2 = 1.0$ in (3) and (7). The image samples generated by the generator after training WAGN-GP are shown in Fig 4.

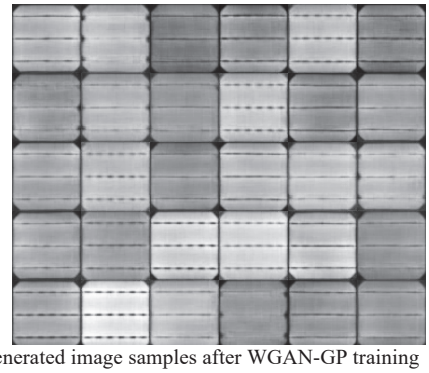

Fig. 4. The generated image samples after WGAN-GP training

In the encoder training phase, using SSIM as the loss function can make the model quickly converge. The curve of the loss function is shown in Fig. 5. Our encoder model has reached a state of convergence after 100 iterations.

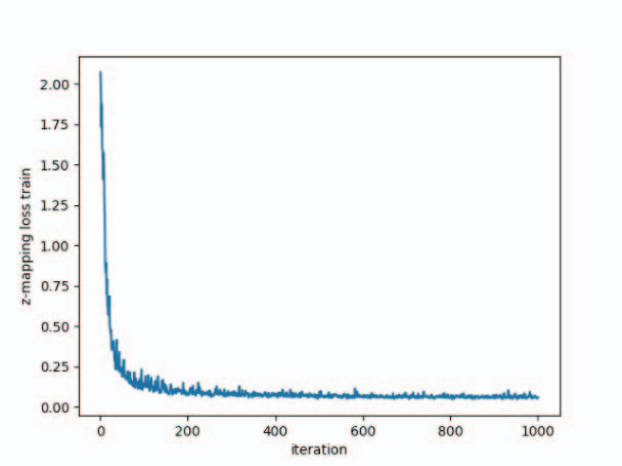

Fig. 5. The curve of the loss function of encoder training

During the encoder training, the ability of the encoder to map images to latent space increases during iteration process, as shown in Fig. 6.

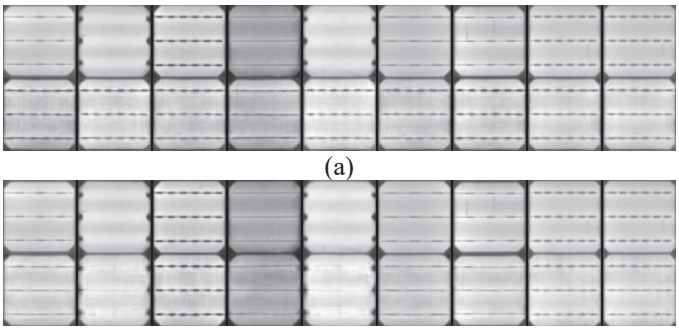

(a)

(b)

Fig. 6. (a)The result of encoder after 50 epochs. (b) The result of encoder after 1000 epochs. First row: origin image samples. Second row: reconstructed image samples from the latent space mapped by the encoder.

In defect detection, we randomly select some normal and abnormal images for testing and visual presentation. An example of defect detection results is shown in Fig. 7.

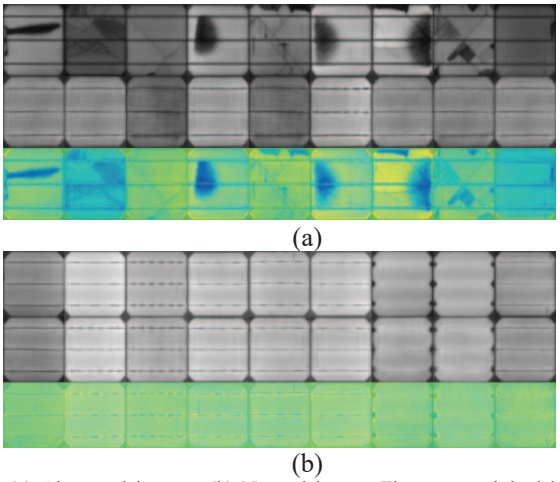

(a)

(b)

Fig. 7. (a) Abnormal images. (b) Normal image. First row: original images. Second row: generated images. Third row: heat map of differences.

The dark parts in the heat map represent areas where anomalies may occur. The darker the color, the greater the possibility of anomalies. It can be seen from the results that our model can detect abnormal areas for abnormal images. For normal images, our model will not detect anomalies.

We next evaluate the impact of using SSIM and MSE as the loss function of the model. We randomly select some normal and abnormal images from the test set and their anomaly score values are shown in Fig. 8. It can be seen that, for anomalous images, the anomaly scores are higher and the anomaly images are better distinguished when using SSIM.

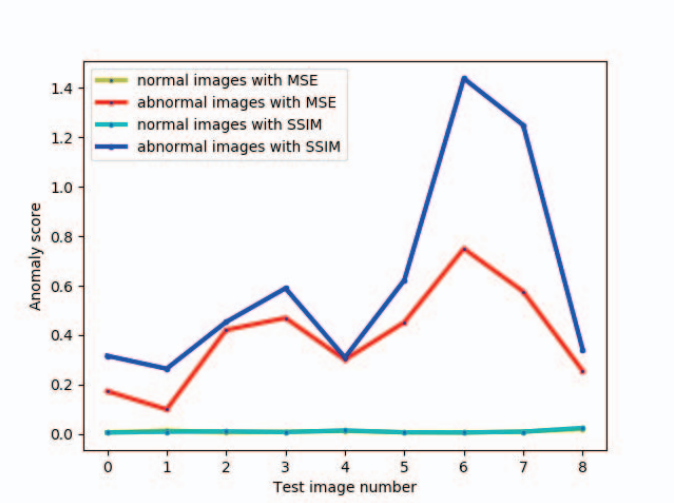

Fig. 8. Test results of model using SSIM and MSE

In order to compare the effects of SSIM and MSE in the training and detection process, we first use MSE with feature residuals as the anomaly score in the detection process and use SSIM and MSE as loss functions in the training process respectively. Table I shows the results of our model on the entire test set using SSIM and MSE in the training process based on the anomaly score with MSE.

TABLE I. TEST RESULTS OF THE TEST SET BASED ON ANOMALY SCORE WITH MSE

	Recall	*Precision*	*F1 Score*
SSIM	85.28	97.27	91.06
MSE	82.23	98.78	89.19

The experiments show that, in training, our model based on SSIM has a higher F1 score than the model based on MSE. And by using SSIM, it can be seen from the higher recall that our model has better detection capabilities for abnormal images.

Then a combination of MSE and SSIM with feature residuals is used as the anomaly score in the detection process and use SSIM and MSE as the loss functions in the training process respectively. Table II shows the results. Our final method achieves detection accuracy of 90.0% on the test set.

TABLE II. TEST RESULTS OF THE TEST SET BASED ON ANOMALY SCORE WITH A COMBINATION OF MSE AND SSIM

	Recall	*Precision*	*F1 Score*
SSIM	89.39	97.67	92.91
MSE	86.87	98.85	92.47

It can be seen from the results that the combination of SSIM and MSE as the abnormal score in the detection phase can improve the F1 score both in the model trained with MSE and SSIM loss function. This shows that SSIM can improve the performance of the model and can measure the difference of images in both global and local aspects. By using SSIM, the model's ability to detect small anomalies is improved. Moreover, our model can locate the abnormal areas by comparing the differences between images. Due to the non-existent iterative process of our model, the detection has high speed and it is suitable for scenarios with high real-time requirements. Because our model adopts the idea of WGAN-GP, our model does not need labeled samples as well as abnormal samples and it is easier to converge in the training.

IV. CONCLUSION

In the present work, an unsupervised model is developed based on GAN and AE with SSIM to detect defects on EL images of solar cells. First, a WGAN-GP is trained with normal images, which contains a generator representing the mapping from latent space to image space and a discriminator. Then the trained WGAN-GP is combined with SSIM to train an encoder, which presents the mapping from the image space to the latent space and measures the differences between the images. In the detection phase, the abnormal areas are detected and located by comparing the differences between the original image and the generated image. The proposed method can solve the problem of insufficient abnormal sample, meet the real-time requirements and has the ability to detect various defects. Compared with MSE, it can reduce effects of the distortion of generated images, making the encoder perform better and obtain better results. Its performance has been verified more effective in comparison with other methods. In the future we expect to speed up the detection process of the model and simplify the model training process. We expect to establish a one-stage detection model that can obtain the inverse mapping during training. Meanwhile, we expect to limit the scope of the latent space to strengthen the stability of the model.

ACKNOWLEDGMENT

This work is supported by Zhejiang Key Research and Development Project (2019C01048).

REFERENCES

[1] Zheng Chai and Chunhui Zhao, “Multiclass Oblique Random Forests With Dual-Incremental Learning Capacity," IEEE Transactions on Neural Networks and Learning Systems, DOI:10.1109/TNNLS.2020.2964737.

[2] Jiang, Yu, Wei Wang, and Chunhui Zhao. "A Machine Vision-based Realtime Anomaly Detection Method for Industrial Products Using Deep Learning." 2019 Chinese Automation Congress (CAC). IEEE, 2019.

[3] Haiyong, Chen, et al. Accurate and robust crack detection using steerable evidence filtering in electroluminescence images of solar cells[J]. Optics and Lasers in Engineering, 2019.

[4] Tsai D M, Wu S C , Chiu W Y . Defect Detection in Solar Modules Using ICA Basis Images[J]. IEEE Transactions on Industrial Informatics, 2013, 9(1):122-131.

[5] Wang C, Jiang X Y, Liu X H . Defect detection in crystalline silicon solar cells based on electroluminescence imaging[J]. Guangdianzi Jiguang/Journal of Optoelectronics Laser, 2011, 22(9):1332-1336.

[6] Tsai D M, Wu S C , Li W C . Defect detection of solar cells in electroluminescence images using Fourier image reconstruction[J]. Solar Energy Materials and Solar Cells, 2012, 99(none):250-262.

[7] Tsai D M, Chang C C , Chao S M . Micro-crack inspection in heterogeneously textured solar wafers using anisotropic diffusion[J]. Image and Vision Computing, 2010, 28(3):491-501.

[8] Anwar S, Abdullah M . Micro-crack detection of multicrystalline solar cells featuring an improved anisotropic diffusion filter and image segmentation technique[J]. EURASIP Journal on Image and Video Processing, 2014, 2014(1):15.

[9] Deitsch S, Christlein V , Berger S , et al. Automatic classification of defective photovoltaic module cells in electroluminescence images[J]. Solar Energy, 2019, 185:455-468.

[10] Zhang L, Yang F , Zhang D , et al. Road crack detection using deep convolutional neural network[C]// IEEE International Conference on Image Processing (ICIP 2016). IEEE, 2016.

[11] Chen F C, Jahanshahi R M R . NB-CNN: Deep Learning-based Crack Detection Using Convolutional Neural Network and Naïve Bayes Data Fusion[J]. IEEE Transactions on Industrial Electronics, 2017, PP (99):1-1.

[12] Jing J, Dong A , Li P , et al. Yarn-dyed fabric defect classification based on convolutional neural network[J]. Optical Engineering, 2017, 56(9):1.

[13] Cha Y J, Choi W. Deep Learning-Based Crack Damage Detection Using Convolutional Neural Networks[J]. Computer-Aided Civil and Infrastructure Engineering, 2017, 32(5):361-378.

[14] Goodfellow I J, Pouget-Abadie J , Mirza M , et al. Generative Adversarial Networks[J]. 2014.

[15] Akcay S, Atapour-Abarghouei A , Breckon T P . GANomaly: Semi-Supervised Anomaly Detection via Adversarial Training[J]. 2018.

[16] Zenati H, Foo C S , Lecouat B , et al. Efficient GAN-Based Anomaly Detection[J]. 2018.

[17] Thomas, Schlegl, Philipp, et al. f-AnoGAN: Fast unsupervised anomaly detection with generative adversarial networks[J]. Medical image analysis, 2019.

[18] Wang Z, Bovik A C , Sheikh H R , et al. Image Quality Assessment: From Error Visibility to Structural Similarity[J]. IEEE Transactions on Image Processing, 2004, 13(4).

[19] Gulrajani I, Ahmed F , Arjovsky M , et al. Improved Training of Wasserstein GANs[J]. 2017.

[20] Zheng Y J, Zhou X H, Sheng W G , et al. Generative adversarial network based telecom fraud detection at the receiving bank[J]. Neural Networks, 2018: S0893608018300698.

[21] Schlegl T, Seeböck, Philipp, Waldstein S M, et al. Unsupervised Anomaly Detection with Generative Adversarial Networks to Guide Marker Discovery[J]. 2017.